Total cross section of the reaction $K^-p \to \bar{K}^0 n$ from 515 to 1065 MeV/c

M. Alston-Garnjost, R. W. Kenney, D. L. Pollard, R. R. Ross, and R. D. Tripp
Lawrence Berkeley Laboratory, University of California, Berkeley, California 94720

H. Nicholson
Mt. Holyoke College, South Hadley, Massachusetts 01075

M. Ferro-Luzzi
CERN, 1211 Geneva 23, Switzerland

(Received 7 September 1977)

We report the results of a precise measurement of the $K^-p \to \bar{K}^0 n$ cross section between 515 and 1065 MeV/c in steps of 10 MeV/c. The statistical errors are less than 1%, a major improvement in accuracy over previous work. We discuss in detail the experimental apparatus and the corrections made to the data. No evidence is found for the new $I = 1$ $\bar{K}N$ resonances at 546 and 602 MeV/c K^- momenta reported recently by Carroll *et al.*

I. INTRODUCTION

In this paper we describe a counter experiment, performed at the Brookhaven National Laboratory Alternating Gradient Synchrotron (AGS), in which we measured with high precision the total cross section (σ_{CEX}) for the charge-exchange (CEX) reaction $K^-p \to \bar{K}^0 n$ between 515 and 1065 MeV/c. Here we elaborate on some of the experimental aspects, describe in detail the corrections to the data, and present the final results. Preliminary values of the cross sections reported previously[1] differ by less than 1% from results reported here. The primary motivation for the experiment was the fact that the low-energy Y^* spectrum is still not as well understood as the corresponding spectrum of N^* resonances, and σ_{CEX} is a valuable indicator of Y^* resonance structure because it is sensitive to the difference between the $\bar{K}N$ $I=0$ and $I=1$ amplitudes. A new partial-wave analysis reported recently[2] has shown that the data we present here are an important new constraint.

The previous measurements of σ_{CEX} in the momentum range between 500 and 1200 MeV/c,[3-6] are shown in Fig. 1 accompanied by three partial-wave predictions.[7-9] Most of these data derive from bubble-chamber experiments of low statistical precision. The first charge-exchange data came from the systematic survey of all K^-p reactions covering the momentum range 435 to 1220 MeV/c performed by the CERN-Heidelberg-Saclay collaboration (CHS).[3] In two bubble-chamber experiments they measured both the differential and the total cross sections for $K^-p \to \bar{K}^0 n$ every 20 MeV/c with statistical accuracy of 30–40% for the differential and 10% for the total cross section. A significant dip appeared at about 740 MeV/c where Berley *et al.*[10] had previously found a narrow resonance in the $K^-p \to \Lambda\eta$ channel just above threshold. Between 900 and 1200 MeV/c a major peak was observed. A subsequent partial-wave analysis[9] identified it as being due primarily to two overlapping resonances: a large one in the F_{05} partial wave and a broad one in D_{15}. Other bubble-chamber experiments followed,[4,5,11,12] improving the level of precision of the σ_{CEX} data above 850 MeV/c. Prior to our experiment the only counter measurements of σ_{CEX} extended from 1 GeV/c upward.[6]

Counter experiments in our momentum range

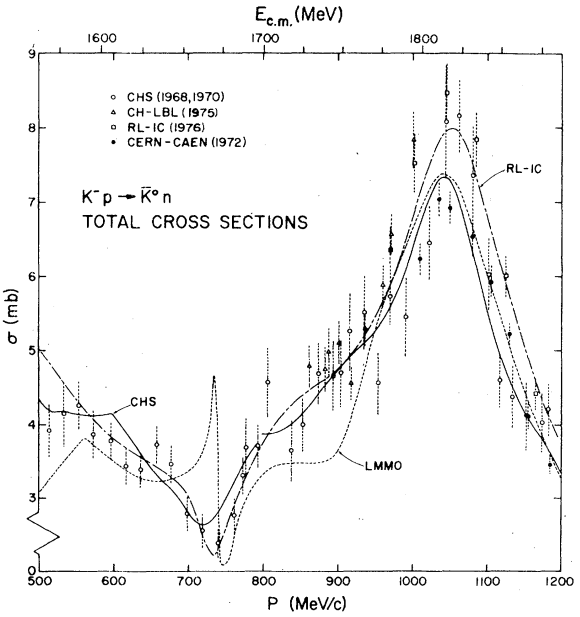

FIG. 1. Measurements of the total cross section for $K^-p \to \bar{K}^0 n$ (Refs. 3–6). The curves are the predictions of three partial-wave analyses (Refs. 7–9).

TABLE I. K^-p final states (other than $K^-p \to K_L n$).

Final states with charged particles	Final states without charged particles
K^-p	$K_S n$, $K_S \to \pi^0\pi^0$
$\Sigma^\pm\pi^\mp$	$\Lambda\pi^0$, $\Lambda \to \pi^0 n$
$\bar{K}^0 p\pi^-$	$\Sigma^0\pi^0$, $\Sigma^0 \to \Lambda\gamma$, $\Lambda \to \pi^0 n$
$\Lambda\pi^+\pi^-$	$K_S n\pi^0$, $K_S \to \pi^0\pi^0$
	$K_L n\pi^0$
$\Sigma^0\pi^+\pi^-$	$\Lambda\eta$, $\Lambda \to \pi^0 n$, $\eta \to$ neutrals
$\Sigma^\pm\pi^\mp\pi^0$	
$\Lambda\pi^+\pi^-\pi^0$	
$\Lambda\pi^0$, $\Lambda \to \pi^- p$	
$\Sigma^0\pi^0$, $\Sigma^0 \to \Lambda\gamma$, $\Lambda \to \pi^- p$	
$K_S n$, $K_S \to \pi^+\pi^-$	
$\Lambda\eta$, $\Lambda \to \pi^- p$	
or $\eta \to$ charged	

measuring cross sections other than σ_{CEX} have been carried out and bear indirectly upon our experimental results through their contributions to partial-wave analyses used in the identification of resonances in the $\bar{K}N$ system. The most recent of these efforts is a BNL measurement[13] made in the new high-intensity K^- beam. Total cross sections for the K^-p and K^-d interactions were reported at closely spaced momentum intervals from 410 to 1075 MeV/c with 1% statistical accuracy. With the use of a Glauber correction to extract the K^-n total cross section from the K^-d cross section, the total cross sections for $I=1$ and $I=0$ states were separately derived. A number of narrow structures in the $I=0$ and $I=1$ total cross sections emerged from this analysis.

The experiment that we report here yielded a precise measurement of the $K^-p \to \bar{K}^0 n$ total cross section (σ_{CEX}) every 10 MeV/c from 515 to 1065 MeV/c with a statistical accuracy of better than 1%. The method used to measure σ_{CEX} was based upon the electronic suppression of all final states, charged and neutral, other than $K^-p \to K_L n$, whose cross section is exactly one-half that of the reaction of interest, $K^-p \to \bar{K}^0 n$. Final states with charged particles (Table I) were vetoed with 100% efficiency by a boxlike array of scintillation counters surrounding the target. Final states, other than $K_L n$, having only neutral particles (Table I) all have at least two and usually four γ rays and were vetoed with high efficiency by a γ-ray detector. The complete veto system thus allows the separation of a nearly pure sample of the reaction of experimental interest, $K^-p \to K_L n$.

In Sec. II we describe the experimental apparatus in more detail; in Secs. III and IV we discuss the data acquisition, analysis, and corrections; in Sec. V we present the final results. A more detailed discussion of the experiment can be found in Ref. 14.

II. EXPERIMENTAL APPARATUS

The experimental arrangement is shown in Fig. 2. We used the momentum-dispersed branch of the Low-Energy Separated Beam ($C2$) (Refs. 15–17) at the BNL Alternating Gradient Synchrotron. After the single stage of separation, the π/K ratio at the target was about 10 over most of the momentum region. The momentum of the beam was established by the first two dipoles, while the momentum spread was adjustable between ±0.5% and ±2.5%. The envelope of the accepted beam was defined by three counters, S_1, M, and S_2. Counter M was the zero-time reference counter for the electronic logic, and counter S_2, located inside a re-entrant hole in the target vacuum system, defined the acceptable beam immediately upstream of the liquid-hydrogen cell.

A Čerenkov counter, located between counters S_1 and M, identified both pions and kaons separately. It was designed and built by T. Kycia and coworkers at BNL and was essential in obtaining a pure kaon beam. Its optics (Fig. 3) included a flat cylindrical radiator that was either Plexiglas or some liquid contained in a glass cell. This geometry selectively captured light of emission angle greater than the critical angle θ_c and reflected it out the periphery into a set of photomultipliers, whose signals provided our "pion signal" C_π. Light having emission angle less than the critical angle θ_c was refracted out of the cell's face and focused onto an adjustable slit. A second set of photomultipliers viewed this slit and

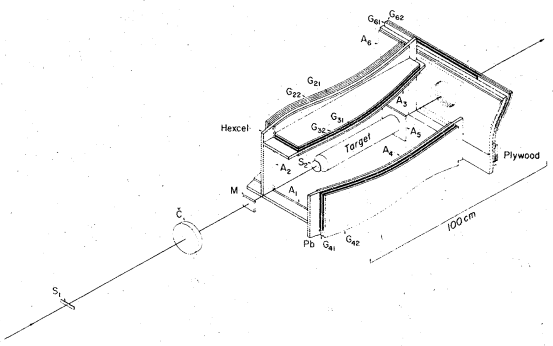

FIG. 2. The counter array surrounding the liquid-hydrogen target.

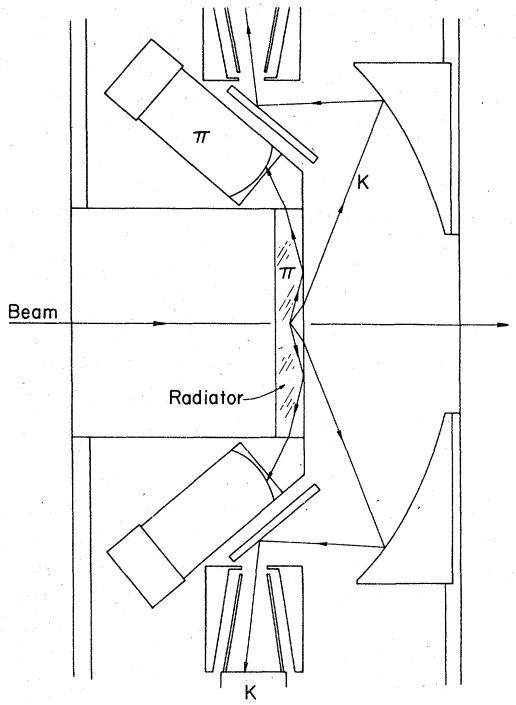

FIG. 3. Schematic of the Čerenkov counter.

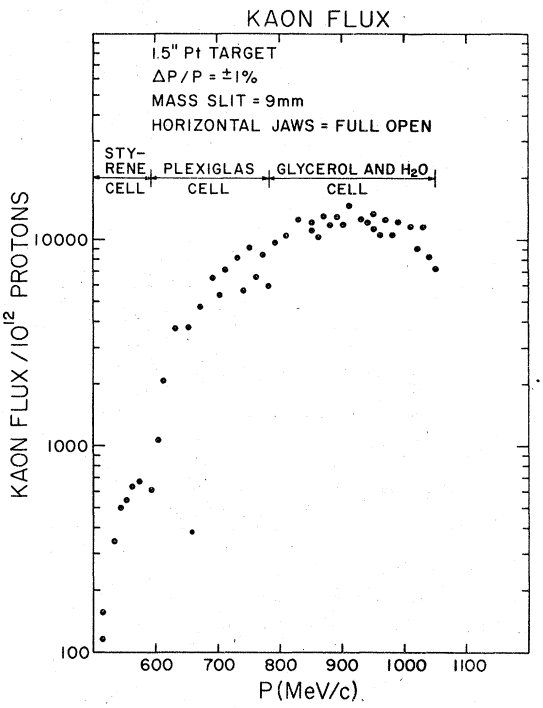

FIG. 4. K^- flux obtained using a 1.5-in. platinum target and $\Delta p/p = \pm 1\%$.

provided our "kaon signal" C_K. The performance of this instrument for various radiators and the resulting purity of our K^- beam are given in Table II.

The beam momentum was established at typical settings by proton, antiproton, and deuteron times of flight over a 6.25-m path beyond the apparatus, and by proton range curves in copper. Both sets of measurements agree to within ±0.5%, which is regarded as the absolute momentum uncertainty. The momentum resolution of the experiment, coming about equally from the momentum spread of the beam and the ionization loss in the target, is nearly constant and averages ±7 MeV/c rms. The lowest beam momentum was determined by our minimum useful K^- flux (Fig. 4) and the upper momentum limit was imposed by the maximum allowable magnet currents.[14]

The liquid-hydrogen target cell was a horizontal cylinder constructed of Mylar and provided with superinsulation. It was 40.8 cm in length and 8.2 cm in diameter, with Mylar end windows 0.006 cm thick. The cylindrical Mylar wall was 0.013 cm thick and the entire cryogenic system was superinsulated by 20 layers of 0.0006-cm aluminized Mylar. The surrounding aluminum vacuum jacket was 0.09 cm thick and was provided with Mylar beam windows at either end that were 0.014 cm thick. The liquid hydrogen was pressurized to 1.12 atm. The hydrogen density was therefore somewhat lower than at 1 atm and was calculated to be 0.0703 g/cm^3.

In order to isolate the reaction $K^-p \to \overline{K}^0 n$, a neutral final state was first defined by an array of

TABLE II. Čerenkov-counter performance. (The kaon detection efficiency was $\approx \frac{2}{3}$.)

Momentum region (MeV/c)	Approximate charged-particle/kaon ratio in the beam	Čerenkov radiator	Radiator index of refraction	Average rejection	Average contamination
515–608	60 to 35	Styrene	1.547	6×10^{-5}	0.3%
598–789	25 to 12	Plexiglas	1.491	2.5×10^{-4}	0.3%
779–1065	15 to 8	Glycerol and H_2O	1.436	3.0×10^{-4}	0.4%

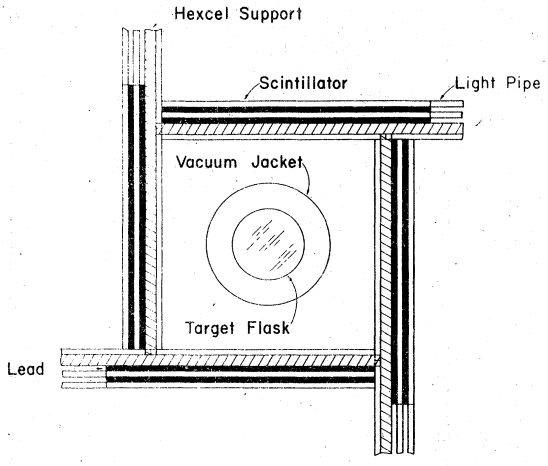

FIG. 5. Schematic end view of the veto counter array.

charged-particle veto counters surrounding the hydrogen target (see Fig. 2). Four counters (A_1 through A_4) formed the lateral portion of an elongated box. The downstream end of the box was closed by another counter (A_6). Counter A_5, just downstream of the target, reduced the background from beamline kaon decays and provided a redundant veto for noninteracting beam particles. Veto inefficiency due to loss of charged secondaries through the open upstream end of the veto box was calculated to be less than 0.3%.

γ-ray detection counters were placed immediately outside of the charged-particle veto counters. Each counter consisted of alternate layers of 0.635-cm-thick lead and scintillator. A front view of this arrangement is shown in Fig. 5. Only two layers each of lead and scintillator were used in order to make the apparatus as transparent as possible to K_L's and neutrons while retaining adequate γ-veto efficiency. A hole in both the lead and scintillator of the counter covering the downstream end of the box allowed passage of the beam and also minimized interactions in the counter due to forward-going neutrons. This hole had only a small effect on the overall veto efficiency for final states having γ rays.

Figure 6 shows the chain of electronic logic used to define the beam flux and charge-exchange candidates. A three-counter coincidence $B = S_1 \cdot M \cdot S_2$ defined the beam geometry. Beam-associated rate dependence was eliminated by a set of veto gates which allowed only those particles that were separated in time from their neighbors by more than 30 nsec to satisfy coincidence BD. An "all quiet" function, AQ, disabled the entire system at ϕ whenever one or more counters in the veto system was producing a signal level greater than 5 mV, thus ensuring that the veto system was always ready when needed. Kaons were identified by the signal from the Čerenkov counter which consisted of a kaon signal with a pion veto. This Čerenkov signal, C, was combined with the rate-independent beam signal, ϕ, to produce the kaon flux signal, $C\phi$.

The anticounters were introduced into the logic in three separate stages. First, A_5, the counter directly after the target, was placed in anticoincidence with the kaon beam signal, ($C\phi$), to provide a measure of the beam-target interactions in the coincidence "interact," (I). Next, the signals from the charged-particle anticounters (A_1, A_2, A_3, A_4, A_6) were combined and used to veto I at the coincidence "neutral final state," (NFS). Last, the signals from all the γ-ray anticounters were added together and the resultant signal used to veto NFS at the final coincidence, Z, the full signature of charge-exchange candidates.

The number of coincidences at B, BD, ϕ, $C\phi$, I, NFS, and Z were counted by scalers, and these numbers formed the data base for the results discussed below.

III. DATA ACQUISITION

At each momentum, the data were accumulated in a series of runs, each consisting of 10^6 kaons

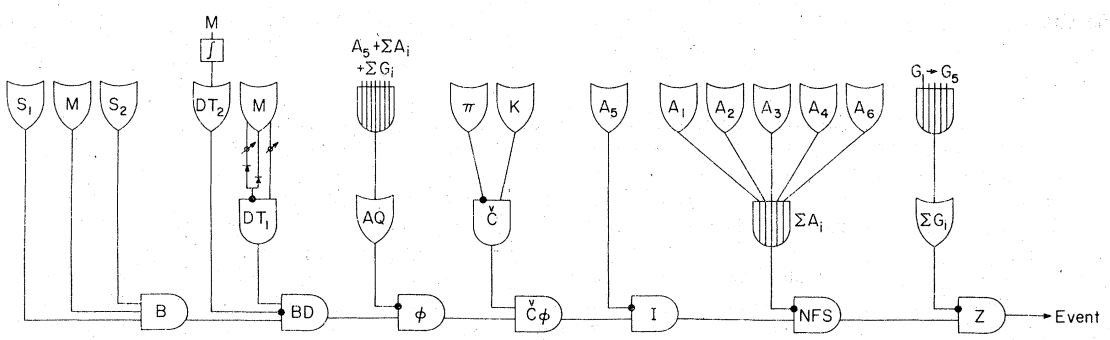

FIG. 6. System electronics.

incident on the target. At each momentum (with a few exceptions near the end of the experiment) runs were taken for both full- and empty-target configurations in order to perform the necessary background subtraction. An attempt was made to accumulate at least 10^7 incident kaons (ten runs) at each momentum, which would give a statistical accuracy of better than 1% for the cross sections, but because of time limitations and the low kaon beam flux, this was not possible at low energies. To check for systematic effects, the runs were first taken every 20 MeV/c (600, 620, 640, etc.), and then the intermediate momenta (610, 630, 650, etc.) were run to give a complete set of measurements spaced every 10 MeV/c. Also, a number of momenta were run twice as a consistency check. No time-dependent effects or systematic shifts or drifts were found. Within statistics the event totals per incident kaon were consistent at the same momentum and smoothly varying from one momentum to another.

IV. CORRECTIONS TO THE EXPERIMENT AND CALCULATION OF σ_{CEX}

Three different types of corrections were calculated for the experiment. First the true K^- path length through the target was determined for full- and empty-target runs from the recorded number of incident kaons corrected for beam contaminants and for attenuation of the beam through the target. Using these corrected path lengths and the measured number of full and empty charge-exchange signatures, a cross section was calculated. From this, subtractions were then made for various deficiencies in the veto system followed by several multiplicative corrections due to final-state interactions and decay of K_L and neutrons. Thus, the equation used to calculate the charge-exchange cross section in millibarns was

$$\sigma_{CEX} = 2\left[\frac{N}{A}\rho L C_1 C_2 C_3 C_4 \left(C_5 C_6 \frac{N_F}{K_F} - \frac{N_{MT}}{K_{MT}}\right) - D_1 - D_2\right] \times C_7 C_8 C_9, \quad (1)$$

where

2 = conversion factor from $K_L n$ events to $\bar{K}^0 n$ events,

$(N/A)\rho L = 583.55$ mb/[event × (incident kaon)],

N_F, N_{MT} = number of events for full- and empty-target runs,

K_F, K_{MT} = number of incident kaons for full- and empty-target runs.

C_i, D_i = corrections discussed below.

Full and empty rates are shown in Fig. 7 as a function of K^- momentum. The empty rates, which varied from 10 to 16 % of the full rates, arise partly from K^- interactions in counter and target materials and partly from the anticipated background from $K_{\mu 2}$ decay muons stopping in the

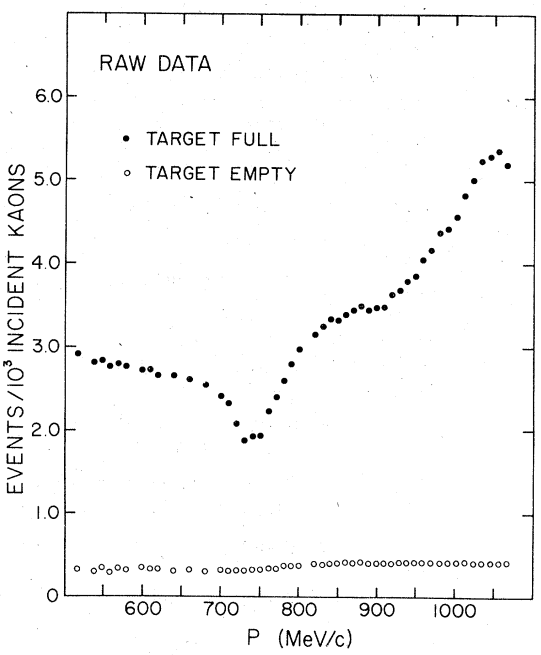

FIG. 7. Raw data used to calculate the total cross section.

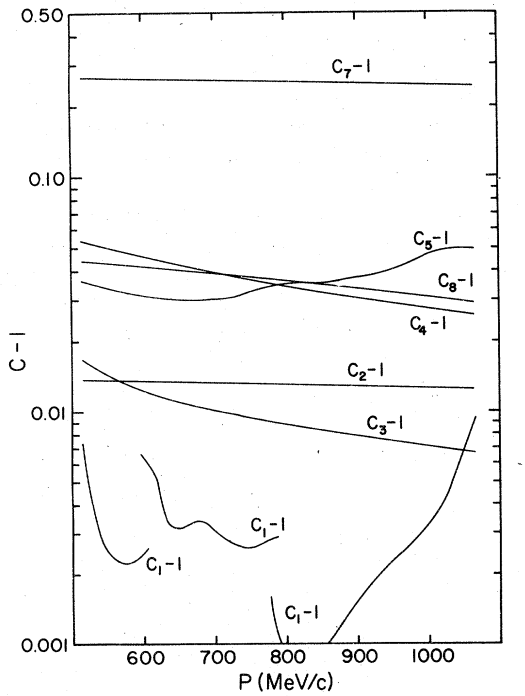

FIG. 8. Multiplicative correction factors discussed in Secs. IV A and IV B.

TABLE III. Corrections to the experiment.

A. K^- path length corrections	C_i	δC_i
C_1 Beam contamination (π, μ, e)	1.001–1.009	0.005
C_2 K^- decays between $\check{C}$ and S_2	1.012–1.014	0.002
C_3 Loss through sides and ends of target	1.007–1.020	0.005
C_4 K^- decays inside the target	1.026–1.054	0.001
C_5 K^- interactions in the target	1.031–1.045	0.004
C_6 δ rays	1.000	0.001
B. Corrections proportional to the $\bar{K}^0 n$ cross section	C_i	δC_i
C_7 K_L and neutron interactions in the target and veto system	1.242–1.265	0.025
C_8 K_L decays inside and outside the veto system	1.029–1.044	0.005
C_9 Undetected K_S decays	1.000	0.002
C. Corrections independent of the $\bar{K}^0 n$ cross section	D_i (mb)	δD_i (mb)
D_1 Unrejected $K_{\mu 2}$ decays	0.031–0.146	0.005
D_2 Unrejected $\Lambda\pi^0$ and $\bar{K}^0 n\pi^0$ final states	0.004–0.039	0.005

target walls. The observed momentum dependence of the empty-target rates is consistent with this interpretation.

The calculated corrections are listed in Table III along with their range of magnitudes and estimated uncertainties, while Figs. 8 and 9 exhibit their momentum dependences. These corrections were calculated by a Monte Carlo program and individually verified by detailed hand calculations. The statistical uncertainties on the corrections coming from the statistics of the Monte Carlo generation were always small compared to those of the experiment itself.

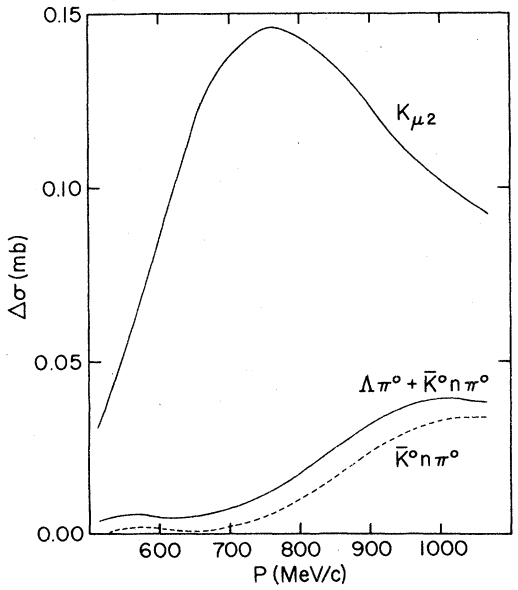

FIG. 9. Subtractive correction factors discussed in Sec. IV C.

A. K^- path length corrections

1. Beam contamination (C_1)

The contaminants of the beam, presumed to be pions, muons, and possibly some electrons, were computed at each momentum. This computation required a knowledge of (i) the rejection (f_π) of non-kaons by the Čerenkov counter, which was measured in a beam free of kaons, (ii) the efficiency (f_K) of the Čerenkov counter for kaon detection, which was measured using a separate time-of-flight particle identification system, and (iii) the ratio ($\phi/C\phi$) of charged particles to identified kaons in the beam. These quantities were measured and are listed in Table II for the various Čerenkov radiators used as is the correction for the non-kaon contamination evaluated by the approximate formula,[14]

$$C_1 = 1 + f_\pi(\phi/C\phi - 1/f_K).$$

The momentum dependence of this correction is

shown in Fig. 8. Discontinuities occur at momenta where the Čerenkov cell was changed. The corrections are seen to be always less than 1%.

2. K^- decays between the Čerenkov counter and counter S_2 (C_2)

After identification of the beam particle as a kaon by the Čerenkov counter, it is possible for it to decay and project one of its charged decay products into the defining counter S_2. This probability was evaluated by Monte Carlo methods for various kaon decay modes. The correction factor C_2 is seen in Fig. 8 to be about 1.3% and virtually independent of momentum.

3. Loss of path length through sides and curved ends of the target (C_3)

Since the defining counter S_2 had a diameter only 2.5 cm smaller than the target, the beam covered a substantial portion of the curved endcaps of the target. Particles displaced from the central axis thus had a slightly reduced path length in hydrogen, especially at low momentum where multiple scattering also contributed to the beam size. In addition, some kaons were multiply scattered out through the sides of the target, further diminishing the path length. Both effects decreased rapidly as the momentum increased, with the combined correction never exceeding 2%.

4. K^- decays within the target (C_4)

The path length available for interactions is reduced due to K^- decays within the target by 2.6% at the highest momentum and 5.4% at the lowest momentum.

5. K^- interactions in the target hydrogen (C_5)

The full-target path length is further diminished by removal of K^- from the beam due to nuclear interactions. Using the total K^-p cross section,[13] this correction was calculated to be about 4%.

6. δ rays (C_6)

A δ ray that penetrates to the veto counters and deposits sufficient energy (400 keV) to produce a signal would veto an otherwise good charge-exchange event. This full-target correction was calculated to be always less than 0.1% even at the highest momentum and was therefore neglected.

B. Corrections proportional to the $\bar{K}^0 n$ cross section

1. K_L and neutron interactions in the target and veto system (C_7)

This is by far the largest correction in the experiment and, because it is so large, dominates the systematic uncertainty in our quoted cross sections. The correction factor is calculated to be about 1.25 and is virtually independent of momentum.

Both particles in a $K_L n$ final state first had to pass through the hydrogen target. Either the K_L or the neutron could interact and produce charged particles, some of which were capable of reaching the veto counters. Using the known Kp and np cross sections,[18] the correction arising from this effect was found to be about 1%, independent of incident kaon momentum.

Next the K_L or the neutron could interact in the lead or the scintillator of the charged-particle or γ veto counters. These interactions are more difficult to analyze because of the lack of information about the details of the interactions of neutrons and K_L's with nuclei. The method used here was a variation of a model developed by Bricman *et al.*[6] for a similar experiment at CERN. For each K_L or neutron, a detection probability is calculated based on the probability of interaction in that material and the probability that an interaction will actually be detected. Finding the interaction probability requires a knowledge of the absorption cross section in carbon and in lead. For neutrons these have been measured and are in good agreement with optical-model calculations.[19] For K_L interactions we used the semiempirical absorption cross section

$$\sigma = 10\pi[R + (\sigma_{K_L N}/10\pi)^{1/2}]^2 \text{ mb}, \qquad (2)$$

where $R = 6.41$ fm for lead and $R = 1.688$ fm for carbon. The K_L-nucleon cross sections, $\sigma_{K_L N}$ (mb), were obtained from the measured $K^{\pm}d$ and $K^{\pm}p$ cross sections[13] above 450 MeV/c and from analysis of bubble-chamber experiments below that momentum.[20] A visibility factor, f_v, as introduced by Bricman *et al.*,[6] was used to represent the fraction of interactions producing a detectable signal in a counter. For K_L interactions in lead and in scintillator and for n interactions in scintillator, we used $f_v = 1$; for n interactions in lead we adopted the parametrization of Bricman *et al.*, $f_v = T_n + 1.11T_n^2$ for $T_n < 0.6$ GeV; $f_v = 1$ for $T_n > 0.6$ GeV, where T_n is the kinetic energy of the neutron.

In order to obtain a correction factor with smooth energy dependence, the angular distributions for charge exchange, required in the Monte Carlo calculation, were obtained from a preliminary version of our partial-wave analysis.[2] This smoothed out the point-to-point fluctuations in the bubble-chamber data. The result was a correction factor nearly independent of momentum varying from 1.24 to 1.26, two-thirds of which came from the interactions of K_L's. The systematic uncertainty in this correction factor was estimated, by varying

visibility factors and interaction cross sections over reasonable ranges, to be ±2.5%.

2. K_L decays inside and outside the veto system (C_8)

About 2% of the K_L's decay inside the veto system with the decay products detected by the veto counters. A comparable number of K_L's decay outside of the veto box and project a decay product back to a veto counter. Monte Carlo studies of the latter were done for all four major K_L decay mode modes.

3. Undetected K_S decays (C_9)

This can occur if the K_S decays outside the veto system or if in the decay $K_S \to \pi^0\pi^0$ none of the resulting four γ's is detected by a veto counter. The probability for such occurrences is calculated to be less than 0.2% and has been neglected.

C. Corrections independent of the $\bar{K}^0 n$ cross section

There are several reactions that were not fully rejected by the veto system. These corrections were independent of the $\bar{K}^0 n$ cross section, but were proportional to the incident K^- flux so that these contributions were subtracted after the flux-corrected cross sections were evaluated, but before corrections related to the $\bar{K}^0 n$ reaction were applied. These veto-system failures were due either to charged particles not reaching the inner layer of counters or to γ rays not being detected in the shower counters.

1. Unrejected $K_{\mu 2}$ decays (D_1)

The only charged-particle veto failure of importance arose when a K^- beam particle decayed between counters S_2 and A_5 through the $K^- \to \mu\nu$ mode and produced a muon of insufficient energy to penetrate to the veto system. This effect was not entirely removed by an empty-target subtraction because of the added stopping power of a full target.

For example, a decay muon originating on the target axis and traveling normal to that axis must have a momentum of 49 MeV/c in order to reach a veto counter under full-target conditions and only 34 MeV/c with an empty target. In our momentum region $K_{\mu 2}$ decay kinematics is such that a substantial number of muons emitted near 180° in the center of mass are affected by such considerations. As can be seen in Fig. 9, the correction for this effect has considerable momentum dependence and becomes as large as 15% of the measured $K_L n$ cross section at 750 MeV/c. However, the calculation of this correction is subject to little uncertainty so the result is known quite precisely.

2. Unrejected $\Lambda\pi^0$ and $\bar{K}^0 n\pi^0$ final states (D_2)

The satisfactory elimination of background reactions having "all-neutral" final states required high efficiency in the γ veto system. The dominant backgrounds came from $K^-p \to \bar{K}^0 n\pi^0$ ($\pi^0 \to \gamma\gamma$) above 800 MeV/c and the four-γ final state of $K^-p \to \Lambda\pi^0$ below 800 MeV/c. The final correction for inefficient photon detection was less than 2% at all momenta. The γ detection efficiency, $P(E)$, of the veto array was estimated using a parametrization developed for this experiment:

$$P(E) = (1 - e^{-nD(E)/l_0\cos\theta})\left(1 - \frac{11.6(l/l_0)^{2.3}}{E^{1.24}\cos\theta}\right), \quad (3)$$

where

l_0 = radiation length of lead (5.6 mm),
n = number of layers of shower counter intersected,
l = thickness of each layer (mm),
$D(E)$ = radiation length/conversion length; $D(E) = 0.77\exp(-4.9E^{-0.622})$, from Ref. 21,
E = energy of photon in MeV,
θ = angle of photon path with respect to normal to plane of the shower counter.

The first factor represents the exponential attenuation of the photons as they produce electron-positron pairs in the lead converter. The second factor is the probability that at least one particle of the pair will emerge from the converter and be detected in the scintillator.[22] The complete expression agrees to within a few percent with efficiencies reported by Darriulat *et al.*[23] for interactions of 30 to 200 MeV photons in up to 10 mm of lead. Nearly all of the photons of interest in this experiment lie in the energy range from 25 to 1000 MeV where the expression is expected to be quite reliable. The average single-γ detection efficiency was found to be approximately 70%, independent of incoming beam momentum.

V. RESULTS AND CONCLUSIONS

The final results for the charge-exchange cross section are listed in Table IV and shown in Fig. 10 as a function of mean laboratory interaction momentum. The errors shown are statistical only and are smaller than 1% over most of the energy region. The systematic uncertainty in overall normalization, coming primarily from the correction for K_L and n interactions in the apparatus, is estimated to be ±3%.

A comparison between the new cross sections and those previously available[3-6] is displayed in Fig. 10, showing the dramatic improvement in accuracy (almost a factor of 10) made by this ex-

TABLE IV. Total cross sections for the reaction $K^-p \rightarrow \bar{K}^0 n$ as a function of incident K^- beam momentum (P_K).

P_K (MeV/c)	σ (mb)	P_K (MeV/c)	σ (mb)
515	4.349 ± 0.076	828	4.363 ± 0.050
536	4.246 ± 0.059	838	4.480 ± 0.026
547	4.188 ± 0.055	848	4.441 ± 0.028
557	4.117 ± 0.055	858	4.532 ± 0.026
567	4.060 ± 0.048	868	4.639 ± 0.015
578	4.012 ± 0.057	878	4.708 ± 0.025
598	3.858 ± 0.049	888	4.643 ± 0.028
608	3.850 ± 0.054	898	4.697 ± 0.026
618	3.711 ± 0.046	907	4.717 ± 0.027
639	3.693 ± 0.044	917	4.957 ± 0.025
659	3.559 ± 0.057	927	5.028 ± 0.036
679	3.438 ± 0.030	937	5.203 ± 0.033
699	3.157 ± 0.039	947	5.302 ± 0.036
708	3.026 ± 0.031	957	5.625 ± 0.038
718	2.590 ± 0.037	968	5.828 ± 0.038
728	2.239 ± 0.022	979	6.177 ± 0.039
739	2.285 ± 0.026	990	6.257 ± 0.039
750	2.300 ± 0.029	1000	6.481 ± 0.041
760	2.759 ± 0.034	1011	6.913 ± 0.037
770	3.051 ± 0.028	1022	7.255 ± 0.043
779	3.315 ± 0.026	1033	7.632 ± 0.048
789	3.658 ± 0.029	1044	7.730 ± 0.045
799	3.929 ± 0.046	1055	7.837 ± 0.037
819	4.189 ± 0.049	1065	7.563 ± 0.043

periment. The agreement between our experiment and bubble-chamber data is exceedingly good below 1 GeV/c. Above that we fall slightly below most of the bubble-chamber data but are significantly higher than the counter results of CERN Caen.[6]

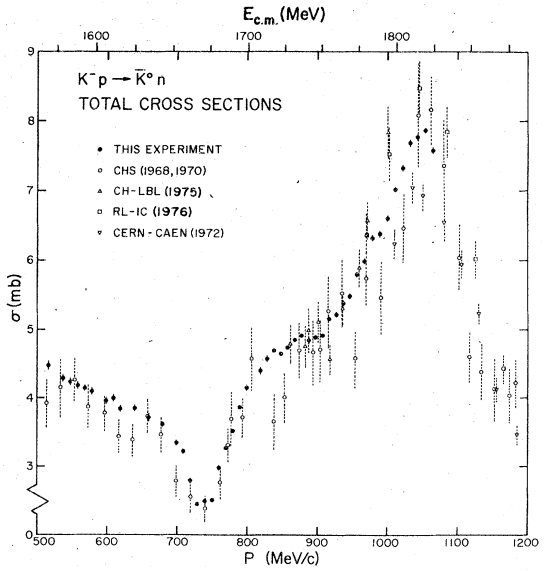

FIG. 10. Comparison between the results of this experiment and previous data (Refs. 3–6).

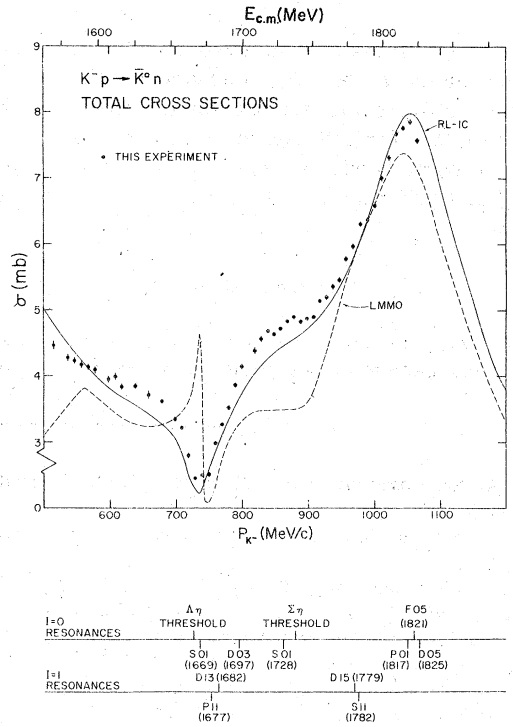

FIG. 11. Comparison between the results of this experiment and two previous phase-shift analyses (Refs. 7 and 8).

The deep U-shaped valley apparent in the cross section in the vicinity of $\Lambda\eta$ threshold (725 MeV/c) is now delineated. The cross section falls rapidly as the threshold is approached from below and appears to be nearly constant immediately above. Beyond that region there is a shoulder more evident than in the bubble-chamber data with a suggestion of a slight dip at $\Sigma^0\eta$ threshold (888 MeV/c). We find no evidence for structure in our charge-exchange cross section between 500 and 600 MeV/c where the results of Carroll *et al.*[13] indicate that the $I=1$ part of the total cross section shows a significant narrow enhancement. A resonance here would be consistent with our lack of structure if it were in a higher partial wave (for example, D_{13} as suggested by Litchfield[24]).

The predictions for the charge-exchange cross section by the two most recent partial-wave analyses appear in Fig. 11. The LMMO solution[7] is incompatible with our data, while the RL-IC solution,[8] although generally in better agreement, fails to reproduce the shoulder between 800 and 900 MeV/c.

We have included these precise σ_{CEX} measurements in a new energy-dependent partial-wave analysis[2] and found that the effects at the $\Lambda\eta$ and $\Sigma^0\eta$ thresholds are well described by cusps.

Also, new values for the masses and widths are found for the P_{01} and P_{11} resonances. Future papers will present our precision measurements of the $K^-p \to \bar{K}^0 n$ differential cross section and a second partial-wave analysis including both the total and differential charge-exchange cross sections.

ACKNOWLEDGMENTS.

We are grateful to the Brookhaven (AGS) staff for their generous assistance and hospitality, to T. Kycia for the loan of the Čerenkov counter, and to T. Mast, J. Nelson, S. Shannon, and D. Neuffer for their assistance in earlier phases of this experiment. We also thank T. Daly, M. Long, and J. Taylor for their technical assistance throughout the experiment. One of us (H.N.) would like to thank the Faculty Grants Committee, the Research Corporation, and the University of Massachusetts Computing Center for financial support. This work was done under the auspices of the U. S. Energy Research and Development Administration, now the Department of Energy.

[1]M. Alston-Garnjost *et al.*, Phys. Rev. Lett. 38, 1003 (1977).
[2]M. Alston-Garnjost *et al.*, Phys. Rev. Lett. 38, 1007 (1977).
[3]CHS (CERN-Heidelberg-Saclay): R. Armenteros *et al.*, Nucl. Phys. B8, 233 (1968); B21, 15 (1970).
[4]CH–LBL (Chicago–Lawrence Berkeley Laboratory): M. Jones *et al.*, Nucl. Phys. B90, 349 (1975).
[5]RL-IC (Rutherford Laboratory–Imperial College): B. Conforto *et al.*, Nucl. Phys. B105, 189 (1976).
[6]CERN-Caen: C. Bricman *et al.*, Phys. Lett. 31B, 148 (1970); C. Bricman, thesis, Université de Paris-Sud Report No. A971, 1972 (unpublished).
[7]LMMO: A. T. Lea, B. R. Martin, R. G. Moorehouse, and G. C. Oades, Nucl. Phys. B56, 77 (1973).
[8]RL-IC: G. P. Gopal *et al.*, Nucl. Phys. B119, 362 (1977).
[9]CHS: R. Armenteros *et al.*, Nucl. Phys. B14, 91 (1969); B8, 195 (1968).
[10]D. Berley *et al.*, Phys. Rev. Lett. 15, 641 (1965).
[11]N. S. Wong, Nuovo Cimento 2A, 353 (1971).
[12]D. F. Kane, Phys. Rev. D 5, 1583 (1972); A. J. Van Horn *et al.*, *ibid.* 6, 1275 (1972).
[13]BNL: A. S. Carroll *et al.*, Phys. Lett. 45B, 531 (1973); Phys. Rev. Lett. 37, 806 (1976).
[14]D. Pollard, thesis, Lawrence Berkeley Laboratory Report No. LBL-5522, 1976 (unpublished).
[15]J. Fox, BNL Accelerator Dept. EP and S Notes No. 7, 1967 and No. 20, 1968 (unpublished).
[16]M. Zeller, BNL Report No. BNL-16000, 193, 1970 (unpublished).
[17]A. Carroll, BNL Accelerator Dept. EP and S Notes No. 54, 1972 and No. 64, 1973 (unpublished).
[18]Particle Data Group Report No. UCRL-20000 NN, 1970 (unpublished); G. A. Sayer *et al.*, Phys. Rev. 169, 1045 (1968); T. Mast *et al.*, Phys. Rev. D 11, 3078 (1975).
[19]J. Franco *et al.*, Phys. Rev. C 6, 748 (1972).
[20]R. D. Tripp, preliminary analysis of LBL Experiment K65 (unpublished).
[21]This is a fit to the curve in Fig. 2.19.4 of B. Rossi, *High Energy Particles* (Prentice-Hall, Englewood Cliffs, New Jersey, 1952), p. 84.
[22]The form of the second factor was suggested by data from the interactions of a tagged photon beam in optical spark chambers with thin (0.08-cm) lead plates. Complete showers were photographed and measured to form a library of shower case histories, and this library, with the aid of a Monte Carlo program, was used to find the energy dependence of photon interaction probabilities, shower penetration depths, and energy depositions. The coefficients in the second term of Eq. (3) were determined by fits in the energy range 50–1000 MeV to the detection efficiencies generated in this manner.
[23]P. Darriulat *et al.*, Nucl. Instrum. Methods 129, 105 (1975).
[24]P. J. Litchfield, Phys. Lett. 51B, 509 (1974).